

# Picosecond Timing with Cherenkov Light in a “Head-on” Geometry

Robert D. Schroll and Henry J. Frisch

June 11, 2004

## Abstract

We discuss the use of Cherenkov radiation produced by a particle traversing the window of a photomultiplier for fast time-of-flight measurements for particle identification. We simulate the production of Cherenkov light in several multi-channel plate photomultiplier tubes and predict the detection of tens of photons per Cherenkov shower. Monte Carlo simulations suggest that time resolutions on the order of 1 ps may be possible with existing devices.

High-energy physics relies on the data produced from colliders. These accelerators intersect counter-rotating beams of particles. Some machines collide protons with protons (Fermilab and LHC), others electrons with positrons (KEK, SLAC Cornell, and Beijing), and others nuclei with nuclei (RHIC). When two particles in opposing beams collide, their combined energy is converted into a shower of secondary particles. By examining the detritus of the collision, experimentalists can determine the intermediate particles formed, and destroyed, in the instants after the collision. Which particles are produced, and how often, gives clues about the basic physics of the standard model.

Identifying the secondary particles is therefore one of the goals of particle detectors, large devices built around the sites where the beams intersect. Typically built in and around a large solenoidal magnet, these detectors consist of various devices to measure the time, position, direction, and energy of the secondary particles. The large magnetic field (typically on the order of 1–2 Tesla), bends the tracks of charged particles, giving a measure of their momentum.

The charged hadrons  $\pi$ ,  $K$ , and  $p$ , the predominant types produced in collisions, have very similar interaction characteristics and can best be distinguished by measurement of their mass. Mass can be measured by combining a velocity measurement with the momentum measurement. This velocity measurement is the goal of time-of-flight (TOF) detectors. Since the secondary particles are typically moving at nearly the speed of light, the time differences between different particles with the same momentum are very small. Figure 1 shows the difference in the time it takes the charged hadrons to travel 1.5 m, as a function of momentum. More accurate mass measurements may also allow the identification of heavy exotic particles which would otherwise be mis-identified as known particles.

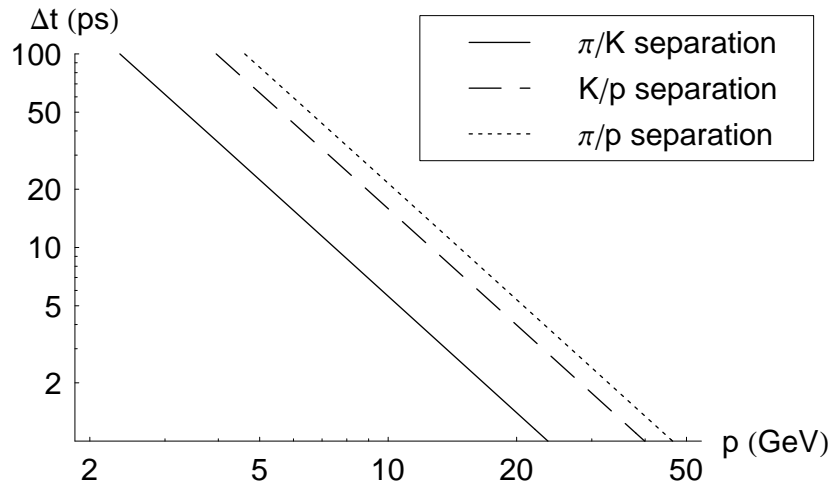


Figure 1: The separations of pions, kaons, and protons, the difference in the time it takes two different particles with the same momentum to travel 1.5 m, as a function of momentum. Current time-of-flight detectors have a time resolution of 100 ps.

## 1 Overview

Current TOF systems typically consist of an array of scintillator bars with photomultiplier tubes (PMTs) at either end. The time resolution of such a system is limited by the difference in path lengths of individual photons traveling down the scintillator to the PMT. Current systems achieve a time resolution of about 100 ps.

We are proposing a different type of TOF system, one in which the particles travel directly through the photodetector itself. This requires that the collision vertex be surrounded by detectors. We propose tiling either the inside (for better timing) or the outside (for better access) of the solenoid with photodetectors [1], as shown in Figure 2. Cherenkov light would be produced in the window of the photodetector, and would shine directly into the detector. Such a setup eliminates both the scintillation and the bouncing of light which limit the time resolution of traditional TOF systems.

We aim to achieve a TOF resolution on the order of 1 ps. To do this, we need photodetectors with superb time resolution. One candidate photodetector for this purpose is a micro-channel plate photomultiplier tube (MCP PMT). Micro-channel plate photomultiplier tubes, shown schematically in Figure 3, resemble traditional PMTs, in that light is converted to electrons by a photocathode, and the electron signal is amplified and deposited on an anode to be detected.

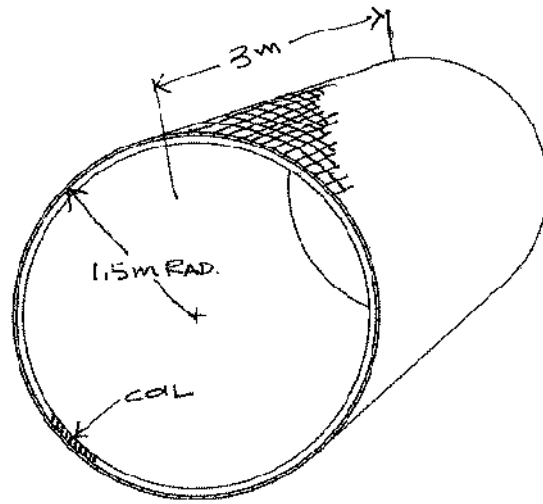


Figure 2: A schematic showing the placement of photodetectors around a detector solenoid coil. The detectors may also be placed just inside of the coil.

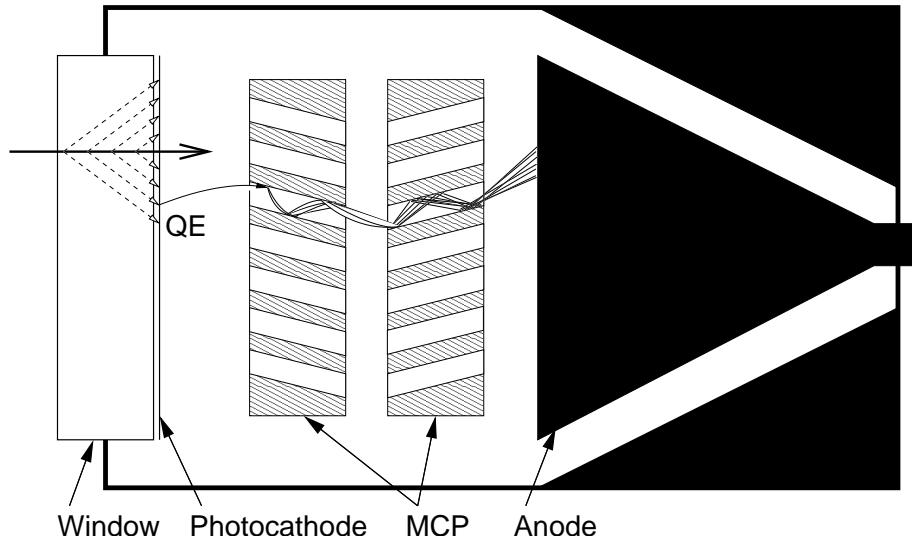


Figure 3: A schematic of the amplification process of a micro-channel plate photomultiplier tube. A relativistic particle produces Cherenkov radiation in the window. This radiation is converted into electrons by a photocathode. The electrons produce a shower in the micro-channel plates, and the shower is deposited on the anode to be detected.

Instead of using a traditional dynode chain for amplification, MCP PMTs use one or more micro-channel plates. Micro-channel plates are lead-glass plates of order 100  $\mu\text{m}$ –1mm thick perforated with an array of cylindrical channels with diameters of 2–100  $\mu\text{m}$ . When a voltage is applied across the plate, each of these channels acts as a dynode chain, giving amplifications of  $10^4$ – $10^7$  [2]. Because of the small channel diameter and compactness of the device, which is only several millimeters thick, electron path lengths through the micro-channel plate cannot vary much, leading to better time resolution.

In addition to TOF measurements, a detector with a 1 ps time resolution could be used to associate photons with collision vertices. When the two beams collide, there may be several individual particle collisions, each of which may produce photons and other particles. Being able to measure the arrival time of the photons to 1 ps would give us sub-millimeter resolution on their path length, helping one to distinguish which collision vertex created which photon.

## 2 Cherenkov Radiation

Cherenkov radiation is produced by a charged particle in a medium when the velocity of the particle exceeds the velocity of light in that medium [3, 4]. Since the velocity of light in a medium is  $c/n$ , where  $n$  is the index of refraction, Cherenkov light will be produced whenever  $v > c/n$ , or using  $\beta \equiv v/c$ ,  $\beta n > 1$ . This radiation is produced essentially instantaneously. In the limit of an infinite radiating medium, it forms a coherent wavefront in the shape of a cone. A little geometry shows that the Cherenkov cone must have an opening half angle of  $\pi/2 - \theta_c$ , where

$$\cos \theta_c = \frac{1}{\beta n} \quad (1)$$

Since we will be studying cases in which the thickness of the radiator is on the order of 1000 times the wavelength of the radiation in question, the infinite radiator approximation is valid.

Cherenkov radiation is ‘blue’; that is, there is more energy in the shorter wavelengths. The number of photons radiated per wavelength per distance is

$$\frac{\partial^2 N}{\partial x \partial \lambda} = \frac{2\pi Z^2 \alpha}{\lambda^2} \left( 1 - \frac{1}{\beta^2 n(\lambda)^2} \right) \quad (2)$$

where  $Z$  is the charge of the particle (in multiples of  $e$ ) and  $\alpha$  is the fine structure constant.[3, 4] Note that the index of refraction generally depends of the wavelength. This corresponds to several hundred photons per centimeter radiated in the visible range. As a rule of thumb, the number of visible photons per centimeter is  $\partial N/\partial x = 400 \sin^2 \theta_c$  [5].

## 3 Detection

Not all of the photons radiated will be detected, however. Some photons, especially those near the edge of the transparency window, may be lost to absorption

in the radiator. Others may reflect off the inside edge of the radiator. More importantly, the photocathode in the photomultiplier will only emit an electron for some fraction of the photons that reach the photocathode. The number of photo-electrons emitted per incoming photon is called the quantum efficiency (QE) of the photocathode, and for most photocathode materials, this number is less than 25% [6].

Two main factors will affect the time resolution of the detector. The first is the spread in the arrival of the Cherenkov radiation to the photocathode. When the charged particle reaches the back edge of the radiator, the radiation produced at the end of its path will also be at the back edge of the radiator. Radiation produced earlier will be spread out in the Cherenkov cone stretching back into the radiator. (See Figure 4.) Working out the geometry, we can show that a photon emitted a distance  $x$  from the rear of the radiator will still have to cover a distance  $d = x(\beta n - 1/\beta n)$  to reach the end of the radiator when the charge particle exits the radiator. Thus, in a radiator of thickness  $T$ , the first photons emitted will arrive

$$\Delta t = \frac{T}{\beta c} (\beta^2 n^2 - 1) \quad (3)$$

after the last photons emitted. Since the photons are emitted uniformly along path of the charged particle, they will arrive uniformly, neglecting absorption, during the interval  $\Delta t$ . Note that, since  $n$  is a function of wavelength,  $\Delta t$  will vary across the spectrum.

The other main factor in the time resolution of the detector is the transit time spread (TTS), or jitter, associated with the photomultiplier tube itself. The time it takes from the creation of a photo-electron to the production of a signal will vary slightly from trial to trial. Some of this variation comes from differences in the path length of the first photo-electron, but much of it comes from difficulties in gathering the signal from all parts of the anode [7]. The best detectors currently on the market have transit time spreads of tens of picoseconds. Burle Industries has developed a 2  $\mu\text{m}$  pore MCP PMT that has achieved a 10 ps TTS [8].

## 4 Sample Detectors

To understand the capabilities of today's state of the art detectors, we have simulated the behavior of some of Hamamatsu's micro-channel plate photomultiplier tubes (MCP PMTs). Five specific models, the R3809U-50, -51, -52, -57, and -58, were selected for study on the strength of their low wavelength behavior. In a custom design, both the material and the thickness of the PMT window can be chosen to optimize performance. However, we use the values cited in a Hamamatsu brochure [9] for the window material and thickness as a starting point for each model. This brochure also includes plots of the quantum efficiency of the detectors versus wavelength. Since these plots are different for detectors with the same photocathode, but different window materials, we see

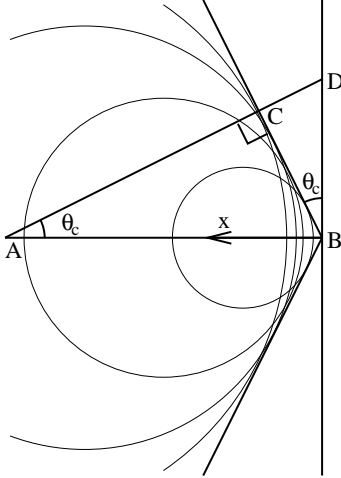


Figure 4: The Cherenkov cone from a charged particle traveling along  $\overline{AB}$  when the particle reaches the edge of the radiator,  $\overline{BD}$ . Light emitted at A still has to travel a distance  $\overline{CD}$  to reach the edge of the radiator. The circles represent spherical wave-fronts emitted from points along the particle's path. The Cherenkov cone forms where these wave-fronts constructively interfere.

that these plots include losses due to the window. Since the Cherenkov light is produced inside the window, not in front of it, we should actually get better detection than predicted. A summary of these detectors is included as Table 1. All of these detectors have a window thickness of 3.2 mm.

Another Hamamatsu document [10] provides an estimate of the TTS of these MCP PMTs. The detectors were exposed to radiation to produce a single photoelectron and the times until signal were plotted in a histogram (Figure 5). Their distribution has a FWHM of 25 ps. While this distribution was not Gaussian,

| Model<br>R3809U- | Spectral Range (nm) |      |      | Photocathode<br>Material | Window<br>Material | Peak<br>QE (%) | Jitter<br>(ps) |
|------------------|---------------------|------|------|--------------------------|--------------------|----------------|----------------|
|                  | Min.                | Peak | Max. |                          |                    |                |                |
| 50               | 175                 | 430  | 850  | Multi-alkali             | Quartz             | 20             | 25             |
| 51               | 175                 | 600  | 900  | EMA <sup>a</sup>         | Quartz             | 8.3            | 25             |
| 52               | 175                 | 400  | 650  | Bi-alkali                | Quartz             | 20             | 25             |
| 57               | 110                 | 230  | 310  | Cs-Te                    | MgF <sub>2</sub>   | 11             | 25             |
| 58               | 110                 | 430  | 850  | Multi-alkali             | MgF <sub>2</sub>   | 20             | 25             |

<sup>a</sup>Extended Red Multi-alkali

Table 1: Some of the characteristics of the Hamamatsu MCP PMTs, taken from [9]. The jitter is the transit time spread (FWHM) for a single photoelectron event.

the main peak was sufficiently close for us to approximate it as such. Thus, in the analysis that follows, we take the transit time spread to be a Gaussian with a FWHM of 25 ps.

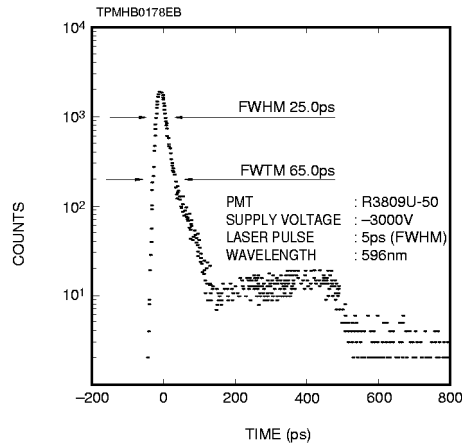


Figure 5: The transit time spread for a single photo-electron event in Hamamatsu’s MCP PMTs (taken from [10]).

## 5 Estimating the Number of Photons

Our first goal was to estimate the number of photons of Cherenkov radiation detected by each PMT. This number will be given by integrating Equation 2 over the thickness of the radiator. For each wavelength, the quantum efficiency must be factored in, and the result can be integrated over the detectable wavelengths to produce the total number of photons detected. Since the particles we plan to investigate have charges of  $\pm e$ , we set  $Z^2 = 1$ . Since the particles will be highly relativistic, we set  $\beta = 1$ . Later, we will estimate the error induced by this.

To estimate the values of  $n(\lambda)$ , we use Sellmeier coefficients for the window materials taken from [11]. These coefficients attempt to fit  $n(\lambda)^2$  to

$$A + \frac{B\lambda^2}{\lambda^2 - C} + \frac{D\lambda^2}{\lambda^2 - E} \quad (4)$$

We found that this fit was good to the fifth decimal place for crystalline quartz, as compared to the experimental values from [12]. For the Model -50, -51, and -52 PMTs, which were listed as having windows of “Quartz (Fused silica or synthetic silica)” [9], we used Sellmeier coefficients for  $\text{SiO}_2$ . The -57 and -58 PMTs have windows of  $\text{MgF}_2$ , which is birefringent. Birefringent materials are given two indices of refraction:  $n_o$ , the ordinary index, and  $n_e$ , the extraordinary index. The ordinary ray, which vibrates perpendicular to the optical axis of the

material, will always travel with an index of refraction  $n_o$ . The index for the extraordinary ray will vary between  $n_o$  and  $n_e$ , depending on the orientation. Since the two indices are rather close in  $\text{MgF}_2$ , we chose to simply use the ordinary index. Since  $n_o < n_e$  in the optical region, this approximation will not overestimate the number of photons produced.

The quantum efficiencies of the photocathodes (with window losses folded in) are given as a plot versus wavelength in [9]. No analytic form, however, was given. We approximated the QE by reading the values at several points and linearly interpolating between them. In the wavelength range 100 nm to 400 nm, where most of the photons will be produced and the QE changes the most dramatically, we sampled the QE every 12.5 nm. Above this range, we sampled only every 25 nm.

The integration of Equation 2 is handled numerically. For each wavelength, the algorithm solves for the number of photons at a distance  $x$  from the front of the radiator (see Figure 4) by Euler’s method, using a step size  $dx$ . (Equation 2 could be integrated exactly for  $x$ ; this method was chosen to allow additional absorption terms to be added.) Once the back edge of the radiator has been reached, the number of photons for each wavelength is multiplied by the quantum efficiency of the photocathode at that wavelength to estimate the number of photons that will actually be detected. The resulting values are integrated over  $\lambda$  using the trapezoidal method with step size  $d\lambda$ .

The number of photons predicted to be detected for each of the five PMTs is listed in Table 2. These integrations were done with step sizes  $dx = 10 \mu\text{m}$  and  $d\lambda = 1 \text{ nm}$ . To test that these step sizes were small enough, we ran an integration with each step size  $1/10$  of the above values. This result differs from the previous result by about 0.02%, which means that our grid size is not causing inaccuracies at a level of concern to us. It is interesting to compare the Model -50 to the Model -58, as they are identical except for their window material. The quartz window of the Model -58 has a higher index of refraction, but is not transparent as far into the ultraviolet as the  $\text{MgF}_2$  window of the Model -58. These data show the extra reach into the ultraviolet more than makes up for the lower index of refraction, so  $\text{MgF}_2$  is the preferred window material.

All of these values were calculated under the approximation  $\beta = 1$ . To test the quality of this approximation, we calculated the number of photons expected for the Model -57 and -58 PMTs for  $\beta$  values ranging from 0.9–1. We found that the percentage change in the number of photons was about twice the change in

|                  |        |        |        |                |                |
|------------------|--------|--------|--------|----------------|----------------|
| Model R3809U-    | 50     | 51     | 52     | 57             | 58             |
| Window Material  | Quartz | Quartz | Quartz | $\text{MgF}_2$ | $\text{MgF}_2$ |
| Photons Detected | 49     | 13     | 47     | 38             | 74             |

Table 2: The number of photons predicted to be detected for each of the PMTs.



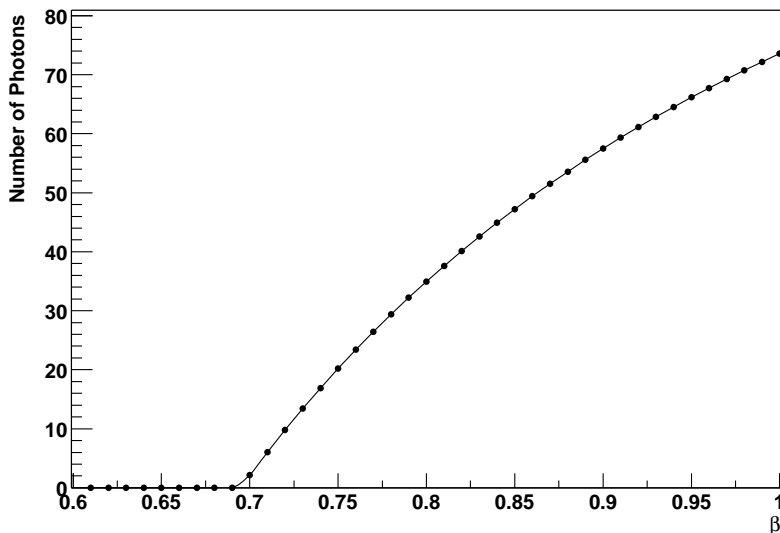


Figure 6: The number of photons detected by the Hamamatsu Model -58 PMT, for varying  $\beta$ . While  $\pi/K/p$  discrimination will take place in the  $\beta = 1$  limit, exotic particles with large mass may be detected at lower  $\beta$ .

$\beta$  (see Fig. 6). This is reasonable, as

$$\frac{1}{N} \frac{\partial}{\partial \beta} \frac{\partial^2 N}{\partial x \partial \lambda} = \frac{1}{\beta} \frac{2}{n^2 \beta^2 - 1} \approx 2 \quad (5)$$

for  $\beta \approx 1$  and  $n \approx 1.5$ . This result provides a simple rule of thumb for estimating effect as  $\beta$  decreases, which is important for searches for heavy exotic particles.

## 6 Estimating the Time Resolution

To estimate the time resolution of MCP PMTs, we developed a Monte Carlo algorithm to simulate the emission and detection of Cherenkov radiation. From these simulations we can estimate the spread in detection times.

The algorithm works by splitting the radiator into a grid in  $x$ , the distance into the radiator, and  $\lambda$ , the wavelength, much like the integration algorithm from above. For each point in the grid,  $\partial^2 N / \partial x \partial \lambda$  was calculated. This was multiplied by the grid size  $dx \cdot d\lambda$  and by the QE for that wavelength. The result was taken to be the probability of emitting a detected photon from that position. A uniform random number on the range (0,1] was generated, and if it was less than the probability from above, a photon was emitted. From Equation 3, the time of arrival at the photocathode after the hypothetical first photon

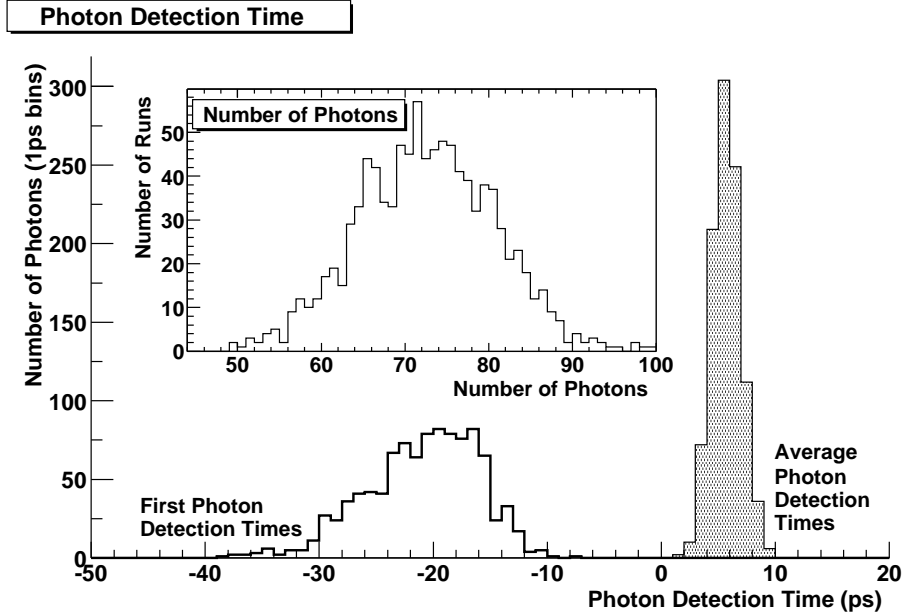


Figure 7: The spread in first photon detection times and average photon detection times for a set of 1000 simulations of Hamamatsu’s R3809U-58. Inset is the number of photoelectrons detected for each of those simulations.

was calculated. A Gaussian random variable, with a mean of 0 and a FWHM of 25 ps, was added to simulate the jitter of the PMT.

Two pieces of information were extracted from the photon detection times: the detection time of the first photon and the mean of the detection times. In a detector, the former would be realized by triggering on the leading edge, while the latter might use a constant fraction trigger. Additionally, we kept track of the total number of photons detected, to assure that the results were consistent with the previous calculations. In order to understand the statistics of the detection times, we ran the simulations many times for each PMT and calculated both the average and root mean squared (RMS) values for the data set. We found that simulation blocks of 1000 runs produced both average and RMS values that differed by around 1%, which is accurate enough for our purposes. Because of the number of runs needed, we used a larger grid spacing than was used for the calculation of number of photons:  $dx = 100 \mu\text{m}$  and  $d\lambda = 10 \text{ nm}$ . One block of runs done with the grid spacing 1/10 as large in both  $x$  and  $\lambda$  produced results that agreed with the looser grid spacing to within 1%.

The results for the five PMTs are summarized in Table 3. In all cases the number of photons generated were distributed in a Gaussian around the value calculated in the previous section. The mean photon detection times also displayed a Gaussian distribution, while the first photon detection times did

| Model               | R3809U-   | 50     | 51     | 52     | 57     | 58     |
|---------------------|-----------|--------|--------|--------|--------|--------|
| First Photon Time   |           |        |        |        |        |        |
|                     | Mean (ps) | -18.83 | -11.91 | -18.49 | -17.85 | -20.84 |
|                     | RMS (ps)  | 5.266  | 6.493  | 5.575  | 5.405  | 5.295  |
| Average Photon Time |           |        |        |        |        |        |
|                     | Mean (ps) | 6.496  | 6.412  | 6.604  | 6.188  | 5.637  |
|                     | RMS (ps)  | 1.682  | 3.129  | 1.691  | 1.922  | 1.347  |

Table 3: The mean and RMS of the first photon detection time and the average photon detection time. Time 0 is the ideal first photon time.

| Transit Time Spread (FWHM) (ps) | 25    | 20    | 15     | 10     | 5      |
|---------------------------------|-------|-------|--------|--------|--------|
| Average Photon Time RMS (ps)    | 1.318 | 1.043 | 0.8374 | 0.6432 | 0.4805 |

Table 4: The variation of the average photon detection time RMS with changing transit time spread of the PMT. All other PMT characteristics are those of the Model -58. Burle Industries has developed a MCP PMT with a TTS of 10 ps. [8]

not. These distributions displayed a long tail toward negative (earlier) times with a sharp cut off on the other side of the peak.

A large component of the spread in the detection times is due to the jitter in the individual photon detection. However, the stochastic nature of both photon emission and photon detection also contributes to the detection time spread. Therefore, while improving the transit time spread of the PMT will improve the overall time resolution, the amount of improvement is limited. Since recent advances have produced PMTs with transit time spread of less than 10 ps [8], we modeled the average photon detection time for a PMT with the same characteristics as Hamamatsu’s Model -58, but with reduced transit time spreads. The results are shown in Table 4. This demonstrates that significant improvement could be made by reducing the transit time spread to 10 ps or less, and that 1 ps resolution is in principle achievable.

## 7 Non-Normal Incidence

Up until this point, we have been assuming that the particle to be detected is moving normal to the surface of the detector. While this greatly simplifies the calculations, it is not representative of the geometry of a particle detector (see Figure 2). Particle paths will be bent by the solenoidal magnetic field of the detector, although, for the high-energy particles in which we are interested, this effect will be minimal. More importantly, the PMTs will not, in general, be directly facing the collision vertex. For the simple arrangement where PMTs are tiled in a cylinder around the beam line, an un-curved track will have an angle of incidence of about  $45^\circ$  for the outer-most PMTs.

We adapted the Monte Carlo algorithm to simulate the emission of Cheren-

kov light from a particle track at an angle of  $\phi$  to the normal. There are two main effects of this change: a longer particle track through the radiator and the loss of azimuthal symmetry. The first is accommodated by increasing the window thickness by a factor of  $1/\cos\phi$ . This allows us to use the same step size as before, which was shown to be small enough to be accurate. To account for the loss of symmetry, each photon generated is randomly assigned an angle  $\psi$ , which represents the angle between the photon's path and the normal plane containing the particle track. As derived in Appendix A, the time delay for a photon emitted a distance  $x$  from the back of the radiator, as measured along the track of the particle, to reach the back of the radiator is given by

$$\Delta t = \frac{x}{\beta c} \left( \frac{\beta^2 n^2}{1 + \cos\psi \tan\phi \sqrt{\beta^2 n^2 - 1}} - 1 \right) \quad (6)$$

It should be noted that, if  $\phi > \theta_c$ , the Cherenkov angle,  $\Delta t$  may run negative for small values of  $\psi$ . Additionally, if  $\phi > \pi/2 - \theta_c$ , photons with  $\psi$  near  $\pi$  will not hit the back face of the radiator. Since these will show up as negative times, care must be taken to determine the legitimacy of negative times.

When  $\phi > \pi/2 - \theta_c$ , there is the possibility that a photon may be emitted nearly parallel to the back face of the radiator. Such a photon would have a very large  $\Delta t$ . Even one such value can greatly disrupt the statistics of the average photon time. Moreover, these photons would not be important for timing: the arrival time, even in an averaging scheme would depend of the initial pulse of photons, not on any stragglers. Therefore, we discard all photon arrival times of more than 150 ps, the rise time of the Hamamatsu MCP PMTs. Since most of the photons arrive in a much shorter window (as shown later; see Figure 8), the total pulse will fall off after about 150 ps. Any photon arriving after that time will not affect the result.

For each in a series of angles  $\phi$ , 1000 simulations were run of the Model -58 MCP PMT, with the same settings used previously. The first photon detection time, the average photon detection time, and the number of photons were collected. The results are listed in Table 5. It should be noted that for  $\text{MgF}_2$   $\theta_c$  is roughly  $\pi/4$ . The RMS of the first photon time is fairly constant for all angles, but the mean shifts significantly for large angles. Using the first photon time would give a constant time resolution, but the shift in the mean would cause a systematic effect if not accounted for. The average photon time gives better time resolution, although this resolution does shift significantly. Also, the average photon time shifts non-monotonically with incident angle, which would also require a correction.

Thus far, we have assumed that all of the photons produced will make it through the interface between the rear of the radiator and the photocathode. In reality, the radiator and photocathode will have different indices of refraction, and only a fraction of the photons, depending on the angle of incidence and polarization, will make it through the interface.

The probability that a photon is transmitted through an interface depends on its polarization. For light polarized in the plane of incidence, the probability

is

$$T_p = \frac{4 n_0 n_1 \cos \theta_0 \cos \theta_1}{(n_1 \cos \theta_0 + n_0 \cos \theta_1)^2} \quad (7)$$

while for polarization perpendicular to the plane of incidence, it is

$$T_s = \frac{4 n_0 n_1 \cos \theta_0 \cos \theta_1}{(n_0 \cos \theta_0 + n_1 \cos \theta_1)^2} \quad (8)$$

where  $n_0$  and  $n_1$  are the indices of refraction and  $\theta_0$  and  $\theta_1$  are the angles of the photon's path to the normal in the two materials [13]. Cherenkov light is polarized in the plane containing the photon and the particle track [14]. Combining these, we find that the probability that a Cherenkov photon is transmitted through the rear interface of the radiator is

$$T = 4 n_0 n_1 \cos \chi \cos \theta_1 \left( \frac{\cos^2 \zeta}{(n_0 \cos \theta_1 + n_1 \cos \chi)^2} + \frac{\sin^2 \zeta}{(n_0 \cos \chi + n_1 \cos \theta_1)^2} \right) \quad (9)$$

where

$$\cos \chi = \cos \phi \cos \theta_c + \cos \psi \sin \phi \sin \theta_c \quad (10)$$

$$\cos \zeta = \frac{1}{\sin \chi} (\cos \phi \sin \theta_c - \cos \psi \sin \phi \cos \theta_c) \quad (11)$$

$$\cos \theta_1 = \sqrt{1 - \frac{n_0^2}{n_1^2} \sin^2 \chi} \quad (12)$$

The details of this calculation are in Appendix B. This probability was added into the Monte Carlo simulation.

The index of refraction of photon cathode materials is, in general, between 2 and 3 [15]. This means that the index of refraction of the photocathode material is greater than the index of refraction of the window material, so there is no chance for total internal reflection. The first photon times, average photon times, and numbers of photons for various angles when  $n_1 = 2.0$  and  $n_1 = 3.0$  are listed in Tables 6 and 7, respectively. There are relatively few differences between the two sets of results, especially for low angles. Since 2.0 is closer to the index of refraction of  $\text{MgF}_2$ , fewer photons are reflected, and the average time RMS is slightly lower in this case, so more photons are detected. Since grazing-incidence photons are more likely to be reflected than normal incidence photons, the average photon time RMS is slightly better in both of these cases than it is for the case with no losses at the interface.

We can also examine the distribution of photon arrival times directly. Figure 8 shows these distributions for various angles of incidence when  $n_1 = 2.0$ . On these plots, the thick curve is a sample data set, and the shaded curve is the average of 100 runs. While individual runs do not have enough data points to give a nice curve, we can see from the average that the parent distribution is mostly Gaussian. As the angle of incidence increases, a slight tail to large times appears, the result of grazing-incidence photons. Since the majority of the photons fall on the Gaussian part of the curve, the 150 ps cut-off discussed before is reasonable.

| Angle<br>( $\pi/2$ ) | First Photon Time |          | Average Photon Time |          | Number of Photons |       |
|----------------------|-------------------|----------|---------------------|----------|-------------------|-------|
|                      | Mean (ps)         | RMS (ps) | Mean (ps)           | RMS (ps) | Mean              | RMS   |
| 0                    | -21.03            | 5.118    | 5.747               | 1.296    | 71.32             | 8.014 |
| 0.125                | -21.02            | 4.945    | 6.124               | 1.275    | 73.46             | 8.095 |
| 0.25                 | -21.22            | 5.089    | 7.639               | 1.464    | 77.86             | 8.528 |
| 0.375                | -21.49            | 4.687    | 12.28               | 2.161    | 84.73             | 8.832 |
| 0.5                  | -22.65            | 4.741    | 15.76               | 3.166    | 85.44             | 9.089 |
| 0.625                | -24.72            | 4.778    | 10.70               | 2.763    | 90.12             | 9.491 |
| 0.75                 | -30.03            | 4.676    | 6.391               | 2.235    | 114.9             | 10.23 |
| 0.875                | -52.37            | 5.402    | -5.436              | 1.943    | 200.7             | 13.28 |

Table 5: Results for a Model -58 PMT with the particle incident at various angles. For each angle, 1000 runs were conducted.

| Angle<br>( $\pi/2$ ) | First Photon Time |          | Average Photon Time |          | Number of Photons |       |
|----------------------|-------------------|----------|---------------------|----------|-------------------|-------|
|                      | Mean (ps)         | RMS (ps) | Mean (ps)           | RMS (ps) | Mean              | RMS   |
| 0                    | -20.58            | 4.913    | 5.740               | 1.320    | 70.65             | 7.900 |
| 0.125                | -20.69            | 4.820    | 6.192               | 1.326    | 72.85             | 8.358 |
| 0.25                 | -21.34            | 5.085    | 4.608               | 1.455    | 75.83             | 8.291 |
| 0.375                | -21.31            | 5.091    | 11.09               | 2.137    | 77.54             | 8.496 |
| 0.5                  | -22.58            | 5.023    | 11.05               | 2.698    | 72.73             | 8.190 |
| 0.625                | -24.56            | 4.780    | 6.685               | 2.282    | 76.15             | 8.537 |
| 0.75                 | -30.34            | 4.965    | 2.106               | 1.991    | 95.84             | 9.562 |
| 0.875                | -52.22            | 5.192    | -10.52              | 1.630    | 165.3             | 12.57 |

Table 6: Results for various angles of incidence with reflection losses included.  $n_1 = 2.0$ .

| Angle<br>( $\pi/2$ ) | First Photon Time |          | Average Photon Time |          | Number of Photons |       |
|----------------------|-------------------|----------|---------------------|----------|-------------------|-------|
|                      | Mean (ps)         | RMS (ps) | Mean (ps)           | RMS (ps) | Mean              | RMS   |
| 0                    | -20.84            | 4.969    | 5.758               | 1.368    | 67.83             | 8.091 |
| 0.125                | -20.43            | 4.957    | 6.233               | 1.352    | 69.60             | 7.963 |
| 0.25                 | -20.79            | 5.019    | 7.788               | 1.551    | 72.31             | 8.592 |
| 0.375                | -20.71            | 4.934    | 11.86               | 2.233    | 73.11             | 8.363 |
| 0.5                  | -21.52            | 5.105    | 11.94               | 3.088    | 64.78             | 7.769 |
| 0.625                | -24.25            | 4.929    | 6.721               | 2.572    | 65.14             | 8.175 |
| 0.75                 | -29.69            | 4.969    | 1.355               | 1.966    | 79.39             | 8.647 |
| 0.875                | -51.55            | 5.794    | -11.78              | 1.615    | 136.4             | 11.78 |

Table 7: Results for various angles of incidence with reflection losses included.  $n_1 = 3.0$ .

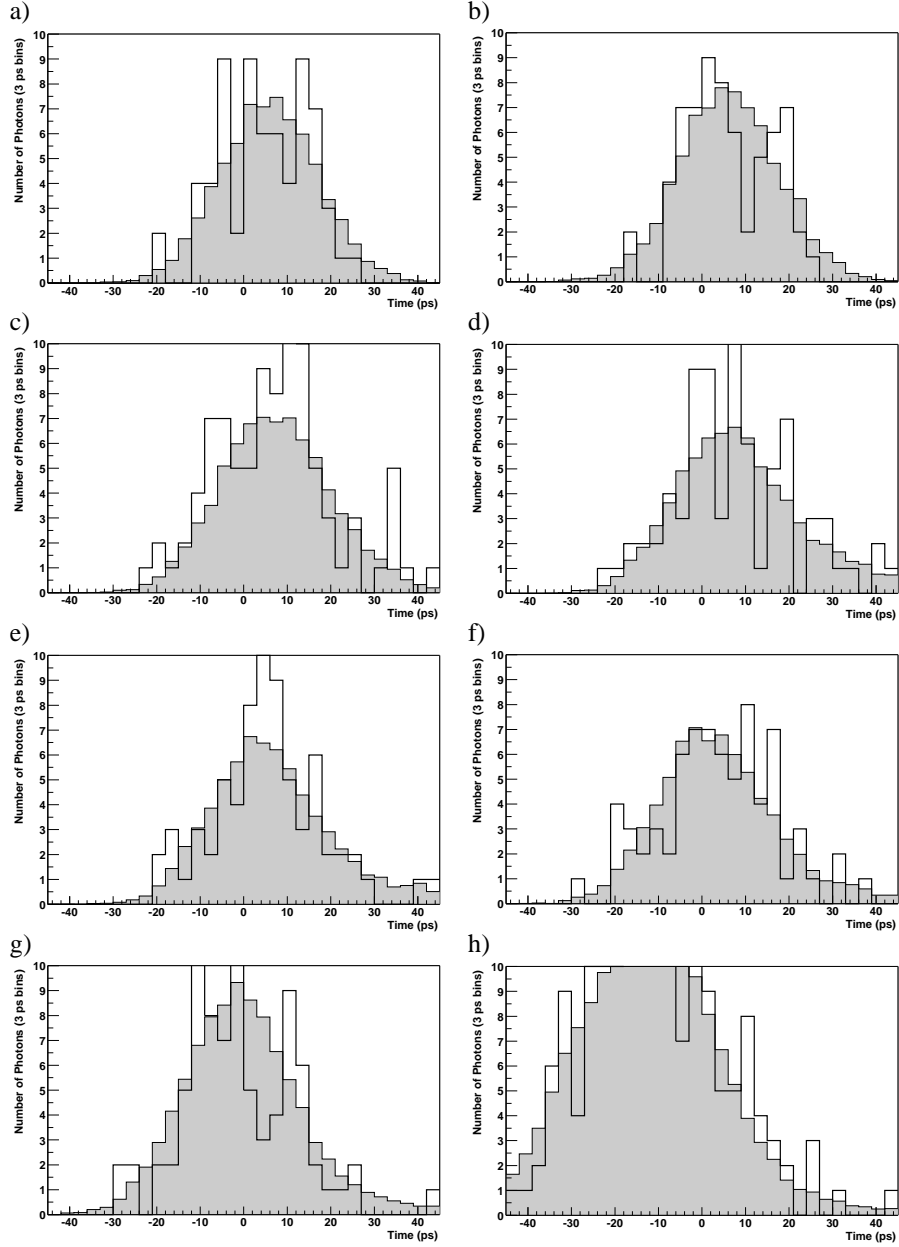


Figure 8: Photon arrival times for the Model -58, with internal reflection for  $n_1 = 2.0$ , for angles of incidence from (a) 0 to (h)  $7\pi/16$ , in steps of  $\pi/16$ . The times are grouped in bins of 3 ps. The thick curve is an example pulse; the shaded curve is an average of 100 sets of data.

## 8 Obstacles

While we have shown that this new time-of-flight system is feasible with current technology, many technical challenges remain.

The current high time resolution MCPs tend to be small; the Hamamatsu MCP PMTs studied have a circular active area with an active area of 11 mm. Larger MCPs have been made, but these have larger pores and do not have the necessary time resolution. Large but fast MCP PMTs must be developed for this system to be feasible.

Micro-channel plate PMTs will probably not function well in the large magnetic fields inside of the detector coil. If placed outside of the coil, the system would also detect showers produced in the coil. For particles moving at an angle to the detector, these showers could potentially trigger the time-of-flight system before the original particle does. This can probably be overcome with a detector sufficiently segmented, so that the particle track can be projected through the coil to a specific element of the time-of-flight system.

If the time-of-flight system is to have picosecond resolution, electronics capable of measuring 1 ps must be developed. This will probably necessitate a custom chip on each MCP PMT. We are investigating the electronics design, which may involve a sub-divided anode with impedance-matched strip lines leading to the output and a “vernier” scheme of mixing the output with a reference signal.

Finally, this system would require thousands of MCP PMTs and would be expensive. We are confident that, if the other problems are overcome, this system would be worth its cost.

## 9 Conclusion

We have proposed a new time-of-flight system in which micro-channel plate photomultiplier tubes surround and look in at the collision vertex. Cherenkov light produced in the MCP PMT windows by the secondary particles is used for detection. Presently, the time resolution of such a system would be limited by the transit time spread of the MCP PMT. With currently available devices, we predict this system could achieve a time resolution near 1 ps. This prediction is based solely on simulations; a physical proof-of-concept test is still needed.

## Acknowledgments

We thank Paul Hink, Bruce Laprade, John Martin, and Wilma Raso, from Burle Industries; Mario Kasahara, from Hamamatsu Corporation, for their assistance on the properties of MCP PMTs. We also thank Alan Bross and Katsushi Arisaka for useful discussions and guidance.

This material is based upon work supported under a National Science Foundation Graduate Research Fellowship. Any opinions, findings, conclusions or



recommendations expressed in this publication are those of the authors and do not necessarily reflect the views of the National Science Foundation.

## A Geometry of Non-normal Incidence

The geometry of non-normal incidence is sketched in Figure 9. Figure 9(a) shows the overview of the situation. The particle is moving along  $\overline{AO}$ , at an angle  $\phi$  to the normal to the back of the radiator (the plane containing  $\overline{OC}$ ). A photon is emitted at point  $A$ , with a path that makes an angle of  $\theta \equiv \theta_c$ , the Cherenkov angle, to the path of the particle. This path is rotated  $\psi$  from the normal to the surface. The photon passes through the plane perpendicular to the particle track at  $B$ , and hits the back of the radiator at  $C$ . We want to find the distance  $\overline{AC}$ .

Figure 9(b) shows the relevant part of Figure 9(a), and Figure 9(c) shows just the plane containing triangle  $AOC$ . Combining the definition  $c \equiv \overline{OB}$  with the definition of  $m$  in 9(b), we see

$$c \sin \alpha = m \cos \phi \quad (13)$$

from which we get

$$\frac{c}{m} = \frac{\cos \phi}{\sin \alpha} = -\frac{\cos \phi}{\cos \psi} \quad (14)$$

Also from Figure 9(c), we get the following relations:

$$c = x \tan \theta \quad (15)$$

$$b = \frac{x}{\cos \theta} \quad (16)$$

$$\ell = b' \sin \theta \quad (17)$$

$$\tan \beta = \frac{m \sin \phi}{c} \quad (18)$$

$$\tan \beta = \frac{y}{L} \quad (19)$$

Plugging Equation 14 into Equation 18, and combining it with Equation 19 gives us

$$\frac{y}{L} = -\tan \phi \cos \psi \quad (20)$$

Next, note that

$$\cot \theta = \frac{x + y}{L} \quad (21)$$

Using Equation 20,

$$\cot \theta = \frac{x}{L} - \tan \phi \cos \psi \quad (22)$$

so

$$L \equiv \ell + c = \frac{x}{\cot \theta + \tan \phi \cos \psi} \quad (23)$$

From Equations 15 and 17, we have

$$b' \sin \theta + x \tan \theta = \frac{x}{\cot \theta + \tan \phi \cos \psi}$$

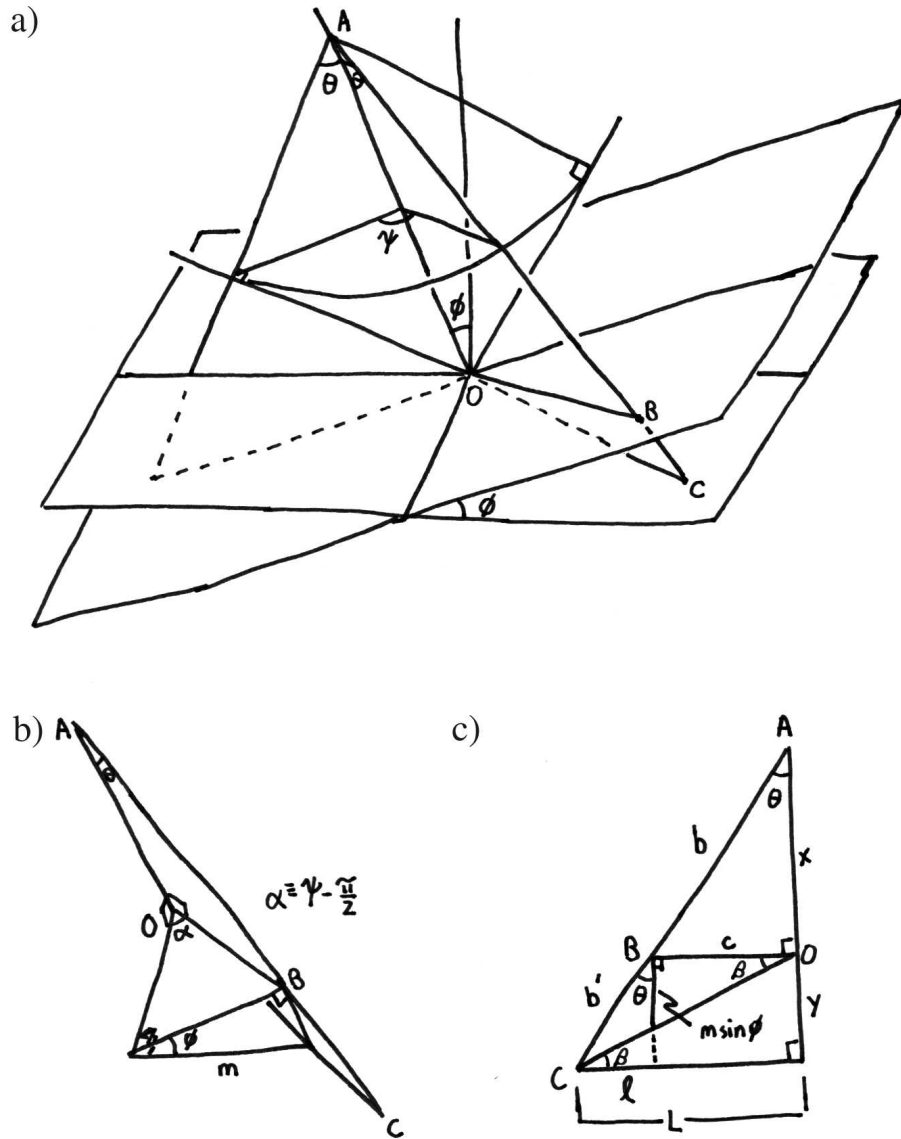


Figure 9: A particle moving along  $\overline{AO}$  emits a Cherenkov photon at  $A$ , which reaches the back of the radiator at  $C$ . We wish to determine the difference between the time when the particle reaches  $O$  and the photon reaches  $C$  in terms of the distance  $x$  and the angles  $\theta$ ,  $\phi$ , and  $\psi$ .

$$\begin{aligned}
b' &= \frac{x}{\sin \theta} \left( \frac{x}{\cot \theta + \tan \phi \cos \psi} - \tan \theta \right) \\
b' &= \frac{x}{\cos \theta} \left( \frac{1}{1 + \cos \psi \tan \phi \tan \theta} - 1 \right)
\end{aligned} \tag{24}$$

Adding Equation 16, we have

$$b + b' = \frac{x}{\cos \theta} \left( \frac{1}{1 + \cos \psi \tan \phi \tan \theta} \right) \tag{25}$$

The particle is moving at a velocity of  $c\beta$ , so it will take a time  $x/c\beta$  to reach the back edge of the radiator. The photon, however, is moving at a velocity of  $c/n$ , so it will take  $(b + b')n/c$  to reach the back of the radiator. Using Equation 1 for  $\cos \theta$ , we find the time difference to be

$$\Delta t = \frac{x\beta n^2}{c} \left( \frac{1}{1 + \cos \psi \tan \phi \tan \theta} \right) - \frac{x}{c\beta} \tag{26}$$

which simplifies to

$$\Delta t = \frac{x}{\beta c} \left( \frac{\beta^2 n^2}{1 + \cos \psi \tan \phi \sqrt{\beta^2 n^2 - 1}} - 1 \right) \tag{27}$$

## B Transmission of Cherenkov Light

The transmission of light at an interface depends on its polarization. Consider Figure 10: a light ray is incident on the interface between a material with index of refraction  $n_0$  and a material with index of refraction  $n_1$ . The plane of incidence is the plane of the paper. The angles  $\theta_0$  and  $\theta_1$  are related by Snell's Law:

$$n_0 \sin \theta_0 = n_1 \sin \theta_1 \tag{28}$$

If the light is polarized so that the electric field points in the plane of incidence, as shown by the  $E_p$  vectors, the intensity transmission coefficient, the fraction of the energy to be transmitted, is

$$T_p = \frac{4 n_0 n_1 \cos \theta_0 \cos \theta_1}{(n_1 \cos \theta_0 + n_0 \cos \theta_1)^2} \tag{29}$$

When the electric field is polarized perpendicular to the plane of incidence, as shown by  $E_s$ , the intensity transmission coefficient is

$$T_s = \frac{4 n_0 n_1 \cos \theta_0 \cos \theta_1}{(n_0 \cos \theta_0 + n_1 \cos \theta_1)^2} \tag{30}$$

These expressions are derived in [13]. Since each photon carries a certain amount of energy, these coefficients are also the probability for the transmission of a photon with one of the polarizations.

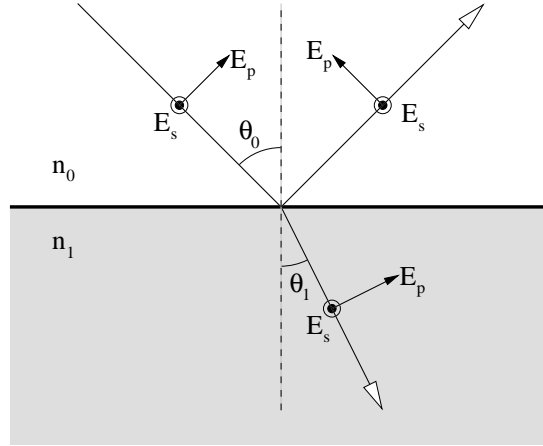


Figure 10: A ray of light is incident on the interface between two materials with different indices of refraction. The amount of light reflected and the amount transmitted depends on if the electric field is in the plane of incidence ( $E_p$ ) or normal to the plane of incidence ( $E_s$ ).

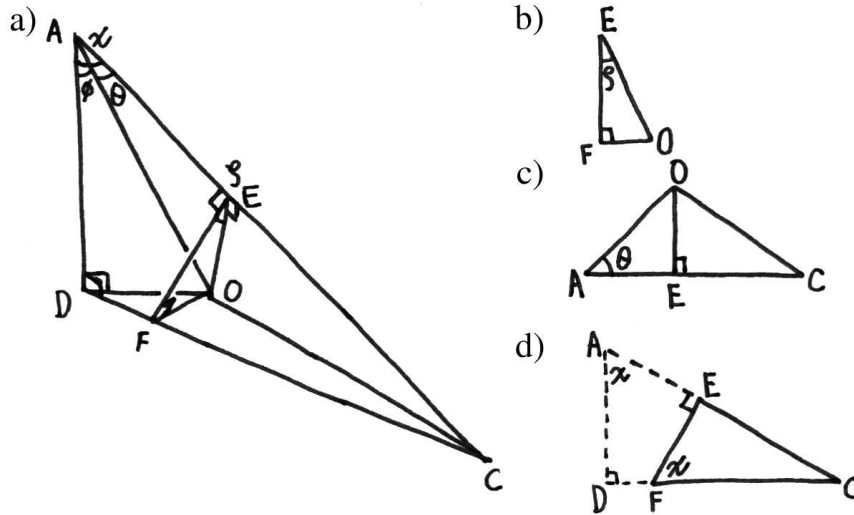


Figure 11: The relevant geometry for determining the probability of a photon being transmitted at the interface between the radiator and the photocathode. The particle is traveling along  $\overline{AO}$  and emits a Cherenkov photon along  $\overline{AC}$ . The photon is polarized with the electric field parallel to  $\overline{EO}$ .  $\chi \equiv \angle DAC$  and  $\zeta \equiv \angle FEO$ .

The geometry of non-normal incidence is sketched in Figure 11. As in Figure 11, the particle travels along  $\overline{AO}$ , emitting a Cherenkov photon that travels along  $\overline{AC}$ .  $\triangle DOC$  lies in the rear plane of the radiator, and  $\overline{AD}$  is a normal to this surface. Thus,  $\triangle ACD$  lies in the plane of incidence.  $\theta$  and  $\phi$  are defined as before;  $\chi$  is used as the angle of incidence. As in Figure 9,  $\overline{AO} = x$  and  $\overline{AC} = b + b'$ . Thus,

$$\begin{aligned}\cos \chi &= \overline{AD}/\overline{AC} \\ &= \frac{x \cos \phi}{b + b'} \\ &= x \cos \phi \frac{\cos \theta}{x} (1 + \cos \psi \tan \phi \tan \theta) \\ \cos \chi &= \cos \phi \cos \theta + \cos \psi \sin \phi \sin \theta\end{aligned}\tag{31}$$

Also, from Snell's Law, we find

$$\sin \theta_1 = \frac{n_0}{n_1} \sin \chi\tag{32}$$

Cherenkov radiation is polarized with the electric field in the plane with the particle track [14]. Therefore, a Cherenkov photon will be polarized parallel to the line  $\overline{EO}$ , at an angle of  $\zeta$  to the plane of incidence. In quantum mechanics, the probability of measuring a particle in some state to be in a given eigen-state is proportional to the square of the inner product of the two states. Thus, the photon will resolve into the  $p$  state with probability  $\cos^2 \zeta$  and be in the  $s$  state with probability  $\sin^2 \zeta$ . The probability for the photon to be transmitted is

$$T = T_p \cos^2 \zeta + T_s \sin^2 \zeta\tag{33}$$

From Figure 11(c), with  $\overline{AO} = x$ , we have

$$\overline{EO} = x \sin \theta\tag{34}$$

$$\overline{AE} = x \cos \theta\tag{35}$$

Figure 11(d) gives us

$$\tan \chi = \overline{CE}/\overline{EF}\tag{36}$$

Since

$$\overline{CE} = \overline{AC} - \overline{AE} = b + b' - x \cos \theta\tag{37}$$

we get

$$\overline{EF} = \frac{1}{\tan \chi} (b + b' - x \cos \theta)\tag{38}$$

From Figure 11(b),

$$\begin{aligned}\cos \zeta &= \overline{EF}/\overline{EO} \\ &= \frac{1}{x \sin \theta \tan \chi} \left[ \frac{x}{\cos \theta} \left( \frac{1}{1 + \cos \psi \tan \phi \tan \theta} \right) - x \cos \theta \right]\end{aligned}$$

$$\begin{aligned}
&= \frac{1}{\cos \theta \sin \theta \tan \chi} \left[ \frac{1 - \cos^2 \theta (1 + \cos \psi \tan \phi \tan \theta)}{1 + \cos \psi \tan \phi \tan \theta} \right] \\
&= \frac{\cos \chi \cos \phi \cos \theta}{\cos \theta \sin \theta \sin \chi} \left[ \frac{1 - \cos^2 \theta - \cos \psi \tan \phi \sin \theta \cos \theta}{\cos \phi \cos \theta + \cos \psi \sin \phi \sin \theta} \right] \\
&= \frac{\cos \phi}{\sin \theta \sin \chi} (\sin^2 \theta - \cos \psi \tan \phi \sin \theta \cos \theta) \\
\cos \zeta &= \frac{1}{\sin \chi} (\cos \phi \sin \theta - \cos \psi \sin \phi \cos \theta) \tag{39}
\end{aligned}$$

Combining Equation 33 with Equations 31, 32, and 39, we get the result quoted in Section 7.

## References

- [1] Micro-channel plates will probably experience problems in the strong transverse magnetic field inside of the solenoid. Outside of the solenoid, showers from the coil could produce early times, if the particle is moving at an angle to the normal of the detector cylinder.
- [2] L. D. Wiza, *Nuclear Instruments and Methods* 162, 587–601 (1979).
- [3] K. Kleinknecht, *Detectors for Particle Radiation, 2<sup>nd</sup> Edition*, University Press, Cambridge (1998).
- [4] W. Leo, *Techniques for Nuclear and Particle Physics Experiments*, Springer-Verlag, New York (1994).
- [5] W. Galbraith, Čerenkov Counters, from W. Galbraith and W. S. C. Williams, eds., *High Energy and Nuclear Physics Data Handbook*, National Institute for Research in Nuclear Science and Rutherford High Energy Lab, Chilton (1969).
- [6] D. Perkins, *Introduction to High Energy Physics*, Addison-Wesley Publishing, Menlo Park (1987).
- [7] K. Arisaka, private communications.
- [8] P. Hink, private communications.
- [9] Hamamatsu Corporation, *2002 Catalog Excerpts: MCP (Microchannel Plate) - PMTs*, [http://usa.hamamatsu.com/assets/pdf/catsandguides/PMTCAT\\_special\\_mcp-pmt.pdf](http://usa.hamamatsu.com/assets/pdf/catsandguides/PMTCAT_special_mcp-pmt.pdf)
- [10] Hamamatsu Corporation, *Microchannel Plate - Photomultiplier Tube (MCP-PMTs) R3809U-50 Series*, [http://usa.hamamatsu.com/assets/pdf/parts\\_R/R3809U-50.pdf](http://usa.hamamatsu.com/assets/pdf/parts_R/R3809U-50.pdf)
- [11] G. Ghosh, *Handbook of Thermo-Optic Coefficients of Optical Materials with Applications*, Academic Press, San Diego (1998).
- [12] W. Wolfe, Properties of Optical Materials, from W. Driscoll and W. Vaughan, eds., *Handbook of Optics*, McGraw-Hill, New York (1978).
- [13] J. Bennett and H. Bennett, Polarization, from W. Driscoll and W. Vaughan, eds., *Handbook of Optics*, McGraw-Hill, New York (1978).
- [14] M. Döring, K. Bernlöhr, et al, *Proceedings of the ICRC 2001* 2985 (2001).
- [15] J. Martin, private communications.